Finite-element simulation of incompressible fluid flow in an elastic vessel

Harry Y. H. Chen[†] and Tony W. H. Sheu[*,‡]

Department of Engineering Science and Ocean Engineering, National Taiwan University, 73 Chou-Shan Road, Taipei, Taiwan, Republic of China

SUMMARY

Finite-element simulation was performed to predict the incompressible Navier–Stokes flow in a domain, partly bounded by an elastic vessel, which is allowed to vary with time. Besides satisfying the physical conservation laws, both surface and the volume conservation laws are satisfied at the discrete level for ensuring the balance between physical and geometrical variables. Several problems which are amenable to analytical solutions were tested for validating the method. The simulated results are observed to agree favourably with analytical solutions. Having verified the applicability of the finite-element code to problems involving moving grids, we consider an incompressible fluid flow bounded by rigid and elastic vessel walls. Our emphasis was placed on the validation of the formulation developed within the moving-grid framework. Copyright © 2003 John Wiley & Sons, Ltd.

KEY WORDS: incompressible; Navier–Stokes flow; elastic; surface and volume; conservation laws; moving grids

1. INTRODUCTION

During the cardiac cycle the change in vessel diameter is observed to be approximately 5–10% in most of the healthy major arteries [1]. In some diseased vessels, the arteries are, however, less compliant and can be treated as being rigid. Flow motion due to the opening/closing of aortic heart valves is a typical example which involves a much larger deformation than that seen in the large arteries [2]. In those problems, the solid structure is driven by the motion of a fluid and, in turn, the fluid domain that moves with time. Under these circumstances, nodes where the solutions are to be evaluated change their co-ordinate values at every time on the boundary as well as in the flow interior. The necessity of taking into account the deformable physical boundary, which is part of the solution procedures, adds

---

* Correspondence to: Tony W. H. Sheu, Department of Engineering Science and Ocean Engineering, National Taiwan University, 73 Chou-Shan Road, Taipei, Taiwan, Republic of China.
† Ph.D. candidate.
‡ E-mail: twhsheu@ntu.edu.tw

modelling complexity and computational difficulty. To develop a theoretically rigorous fluid–structure model for modelling flows in deformable domain is the main objective of the present study.

The fluid–structure interaction problem can be numerically analysed by global and coupled approaches [3]. In 1989, Peskin and McQueen [4] proposed the first global approach, known as the immersed boundary method. As the name indicates, the structure is considered as the immersed solid, allowing us to consider Navier–Stokes equations in the whole fluid–structure domain. Since the solid immersed in the fluid is modelled by a momentum forcing term in the Navier–Stokes equations, this method is applicable to model complex geometry problems on orthogonal grids. The advantage is that the moving-boundary problems can be tackled straightforwardly without resorting to mesh regeneration with time [5]. Both computing resources (memory and CPU time) and man hours can be considerably saved. The distributed Lagrange–multiplier method is another class of global approaches. In the fictitious domain, the rigid-body motion of a structure is constrained by the employed Lagrange multiplier [6], which is considered as the body force to maintain the rigid-body motion. The immersed interface method [7] is one of the well-known variants of the immersed boundary method.

The underlying idea of constructing a coupled approach is to couple the flow model with the structure model through some suitable matching conditions. Amongst of this class of methods, the arbitrary Lagrangian–Eulerian (ALE) [8] and space–time methods [9] are often referred to. On physical grounds, the fluid phase is described in Eulerian co-ordinates and the Lagrangian formulation is more appropriate for use in the solid phase. These two formulations are, however, incompatible. In the early 1980s, Hughes *et al.* [10] and Donea [8] combined the nice features of each formulation in their ALE finite-element simulations of fluid structure interaction. This combined model is manifested by a continuous adapt ion of the mesh and requires, in theory, no time-consuming mesh regeneration. Under the large deformation conditions, a mesh of good quality is difficult to maintain without considerable remeshing. The dispensable interpolation of field variables on the newly updated mesh may introduce artificial diffusivity, in particular for large deformation problems. The added error to the formulation can even make the ALE method unstable. The fictitious domain/mortar element has been proposed to resolve this difficulty [11, 12]. This class of methods solves the flow equations in Eulerian description in a fixed mesh and analyses the structure equations in a Lagrangian setting. As said earlier, the velocity constraint associated with the rigid internal boundaries is imposed by means of the Lagrange multiplier.

The space–time finite-element method is another class of moving methods for solving moving-boundary problems. This method, firstly proposed by Hughes and Hullbert [9] in solving the elastic-dynamic problem, approximates the temporal derivative using the finite-element method. The advantage of this method is its generality. One can view the ALE finite-element model as a special case of the space–time model, as discussed by Hansbo [13] and Behr and Tezduyar [14]. Besides the above two major coupled methods, the recently developed lattice Boltzmann method [15] and the front tracking method [16] are good methods for simulating a large number of solid objects in the flow. One can refer to Hu *et al.* [17] for more information.

We employ in the study the ALE-coupled approach for two reasons. Firstly, physically correct equations governing the fluid and solid are used in their respective domain. In addition, the stability of the ALE finite-element formulation has been theoretically demonstrated [18]. Secondary, use of the coupled approach enables us to split the global computation into a

sequence of computations for the fluid and the structure. A considerable reduction of the computational complexity can be gained. Within the ALE framework, we can derive the conservation equations for the fluid flow in moving co-ordinates through transformation of variables [3]. One can also derive the working equations in moving co-ordinates based on the concept of the Lie derivative [19–21]. The grid fitted to the body moves in time. It is important to satisfy the space conservation law (SCL) for properly relating the change of the cell area to the co-ordinate frame velocity. Failure to satisfy the space conservation law may cause the mass to accumulate or diminish. Thomas and Lombard [22] were among the first to address the necessity of imposing this constraint when analysing the physical conservation equations. Demirdizic and Peric [23] later justified the necessity of satisfying the SCL constraint condition when simulating problems on non-stationary grids. It is trivial that the discrete geometric conservation law (GCL) condition is satisfied in the constant flow case [24]. This requirement, in turn, constrains the geometrical quantities. For additional details, one can refer to References [25, 26].

The remainder of this paper is organized as follows. In the next section, we derive the working equations in the ALE description. Equations which govern the motion of a linearly elastic, incompressible, isotropic vessel are also given. In the following section, we outline the finite-element method and provide analytical verification. This is followed by presenting the simulated results for an incompressible fluid flow in a vessel which partly undergoes a finite-amplitude oscillation. Finally, we offer some concluding remarks.

2. MATHEMATICAL MODELS

The incompressible equations governing a viscous Newtonian fluid flow in grids fixed in space are as follows:

$$\rho \frac{\partial \bar{\Phi}}{\partial t} + \frac{\partial}{\partial x}(\rho \, u \, \bar{\Phi}) + \frac{1}{r^\alpha} \frac{\partial}{\partial y}(r^\alpha \, \rho \, v \, \bar{\Phi}) = \frac{\partial}{\partial x}\left(\Gamma \frac{\partial \bar{\Phi}}{\partial x}\right) + \frac{1}{r^\alpha} \frac{\partial}{\partial y}\left(\Gamma \, r^\alpha \frac{\partial \bar{\Phi}}{\partial y}\right) + S \qquad (1)$$

Provided that $\bar{\Phi} = 1$, $\Gamma = 0$ and $S = 0$, the above equation denotes the continuity equation. As for equations with $\bar{\Phi} = u$ (or v) and

$$S = -\frac{\partial p}{\partial x} + \frac{\partial}{\partial x}\left(\Gamma \frac{\partial u}{\partial x}\right) + \frac{1}{r^\alpha} \frac{\partial}{\partial y}\left(r^\alpha \Gamma \frac{\partial v}{\partial x}\right) \quad \left(\text{or} \; -\frac{\partial p}{\partial y} + \frac{\partial}{\partial x}\left(\Gamma \frac{\partial u}{\partial y}\right)\right.$$

$$\left. + \frac{1}{r^\alpha} \frac{\partial}{\partial y}\left(r^\alpha \Gamma \frac{\partial v}{\partial y}\right) - \frac{2\alpha \Gamma v}{r^2}\right)$$

they stand for the x- and y-momentum equations, respectively. Equation (1) represents the truly two-dimensional equation when $\alpha = 0$ and the angle-independent equation in cylindrical co-ordinates when $\alpha = 1$. For simplicity of presentation the method we consider the following equations written in x–y co-ordinates:

$$\frac{\partial u}{\partial x} + \frac{\partial v}{\partial y} = 0 \qquad (2)$$

$$\frac{\partial u}{\partial t} + u\,\frac{\partial u}{\partial x} + v\,\frac{\partial u}{\partial y} = -\frac{1}{\rho}\,\frac{\partial p}{\partial x} + \frac{\mu}{\rho}\,\left(\frac{\partial^2 u}{\partial x^2} + \frac{\partial^2 u}{\partial y^2}\right) \tag{3}$$

$$\frac{\partial v}{\partial t} + u\,\frac{\partial v}{\partial x} + v\,\frac{\partial v}{\partial y} = -\frac{1}{\rho}\,\frac{\partial p}{\partial y} + \frac{\mu}{\rho}\,\left(\frac{\partial^2 v}{\partial x^2} + \frac{\partial^2 v}{\partial y^2}\right) \tag{4}$$

The above equations involve a velocity vector $\underline{u} = (u, v)$ and pressure p for a fluid flow having a fixed kinematic viscosity μ. One advantage of adopting the primitive-variable formulation is due to its accommodation of closure initial and boundary conditions [27].

It is natural to adapt grid lines to the flow when simulating a moving boundary flow problem. Let (X_1, X_2) and (x_1, x_2) be Lagrangian and Eulerian co-ordinates, respectively. One can represent the material time derivative of a passive scalar ϕ at a given point χ_i in the fluid domain and at a time t as follows ($i = 1$–2):

$$\frac{\mathrm{D}\phi(\chi_i, t)}{\mathrm{D}t} = \frac{\delta\phi(\chi_i, t)}{\delta t} + (u_i - w_i)\frac{\partial\phi(x_i, t)}{\partial x_i} \tag{5}$$

In the above, $\mathrm{D}\phi/\mathrm{D}t$ represents the material derivative of ϕ at a given point X_i. As for $\delta\phi/\delta t(\equiv (\partial/\partial t)\phi(\chi, t)|_{\chi\text{fixed}})$, it stands for the referential time derivative keeping the co-ordinates, χ_i, in the referenced domain constant. In addition, u_i and $(w_i \equiv (\mathrm{d}/\mathrm{d}t)x(\chi, t))$ are known as the material and reference velocities, respectively. Substituting Equation (5) into the unsteady convection–diffusion transport equation for ϕ in Lagrangian description, we can obtain the following equation:

$$\phi_t + (u - w_1)\phi_x + (v - w_2)\phi_y - \frac{\mu}{\rho}(\phi_{xx} + \phi_{yy}) = 0 \tag{6}$$

The reference velocity $w_i(u = 1$–$2)$ can be chosen arbitrarily. If w_i is equal to zero, the above transport equation for ϕ becomes that in the Eulerian description. Note that specification of w_i as the fluid particle velocity renders Equation (6) expressed in the Lagrangian description. Let w_i be the moving gird velocity vector (u_g, v_g), we can express the transport equation in moving grids as

$$\phi_t + (u - u_g)\phi_x + (v - v_g)\phi_y - \frac{\mu}{\rho}(\phi_{xx} + \phi_{yy}) = 0 \tag{7}$$

Guided by the above theoretical basis, we can transform Equations (2)–(4) in fixed grids into their moving co-ordinate counterparts:

$$u_x + v_y = 0 \tag{8}$$

$$u_t + (u - u_g)u_x + (v - v_g)u_y = -\frac{1}{\rho}\,p_x + \frac{\mu}{\rho}\,(u_{xx} + u_{yy}) \tag{9}$$

$$v_t + (u - u_g)v_x + (v - v_g)v_y = -\frac{1}{\rho}\,p_y + \frac{\mu}{\rho}\,(v_{xx} + v_{yy}) \tag{10}$$

Modelling of flow–structure interaction problem is followed by deriving a differential system in a compliant medium, which is subjected to a finite deformation. To simplify the analysis, we

consider that the elastic properties are identical in all directions. The equations of equilibrium for such homogeneous isotropic elastic structures can be derived by invoking the D'Alembert principle and adding the body force $\bar{F}(\equiv F_i, \ i = 1, 2)$ to the inertia force, yielding

$$\tau_{ij,j} + F_i = \rho_w \ddot{d}_i \tag{11}$$

In the above, $\ddot{d}_i$ denotes $\mathrm{d}^2 d_i / \mathrm{d}t^2$, where $\underline{d} = (d_1, d_2)$ and ρ_w are known as the displacement vector and the density of the elastic vessel, respectively. To close the differential system for modelling the wall motion, we consider the following stress–strain relation

$$\tau_{ij} = \lambda \delta_{ij} d_{k,k} + G(d_{i,j} + d_{j,i}) \tag{12}$$

The above constitutive equation involves two Lame's constants (or elastic constants) G and λ. These material constants are, as usual, written in terms of the Young's modulus E and the Poisson ratio $\bar{v}$:

$$G = \frac{E}{2(1 + \bar{v})} \tag{13}$$

$$\lambda = \frac{\bar{v}E}{(1 + \bar{v})(1 - 2\bar{v})} \tag{14}$$

Substituting Equations (12)–(14) into (11), we can obtain the so-called Navier equations for a linearly elastic medium given below [28]:

$$\rho_w \frac{\mathrm{d}^2 d_1}{\mathrm{d}t^2} - \frac{\partial}{\partial x}\left[(\lambda + 2G)\frac{\partial d_1}{\partial x} + \lambda \frac{\partial d_2}{\partial y}\right] - \frac{\partial}{\partial y}\left[G\left(\frac{\partial d_1}{\partial y} + \frac{\partial d_2}{\partial x}\right)\right] = F_1 \tag{15}$$

$$\rho_w \frac{\mathrm{d}^2 d_2}{\mathrm{d}t^2} - \frac{\partial}{\partial x}\left[G\left(\frac{\partial d_2}{\partial x} + \frac{\partial d_1}{\partial y}\right)\right] - \frac{\partial}{\partial y}\left[(\lambda + 2G)\frac{\partial d_2}{\partial y} + \lambda \frac{\partial d_1}{\partial x}\right] = F_2 \tag{16}$$

where F_1 and F_2 are as the prescribed fluid forces. To close the above differential system, we specify $\partial d_i / \partial x_i = 0$, where $i = 1, 2$, at two ends of the elastic material. On physical grounds, stresses are continuous across the interface that separates the incompressible fluid flow and elastic medium. In other words, the elastic stress tensor, $\tau_{ij}(= \lambda \delta_{ij} d_{k,k} + G(d_{i,j} + d_{j,i}))$, should be equal to the flow stress tensor, governed by Stokes constitutive relation, $\tau_{ij} = -p\delta_{ij} d_{k,k} + \mu(u_{i,j} + u_{j,i})$, in a Newtonian fluid. Continuity of stresses between a fluid and an elastic material demands that

$$(\lambda + 2G)\frac{\partial d_1}{\partial x} + \lambda \frac{\partial d_2}{\partial y} = \tau_{xx} \tag{17}$$

$$\lambda \frac{\partial d_1}{\partial x} + (\lambda + 2G)\frac{\partial d_2}{\partial y} = \tau_{yy} \tag{18}$$

$$G\left(\frac{\partial d_1}{\partial y} + \frac{\partial d_2}{\partial x}\right) = \tau_{xy} \tag{19}$$

By definition, the normal stresses (τ_{xx}, τ_{yy}) and shear stress (τ_{xy}) are as follows:

$$\tau_{xx} = -p + 2\mu \frac{\partial u}{\partial x} \tag{20}$$

$$\tau_{yy} = -p + 2\mu \frac{\partial v}{\partial y} \tag{21}$$

$$\tau_{xy} = \mu \left(\frac{\partial u}{\partial y} + \frac{\partial v}{\partial x} \right) \tag{22}$$

On the boundary separating the ambient and the elastic material, we assume that $p = 0$ and $\tau_{xx} = \tau_{yy} = \tau_{xy} = 0$.

The Navier–Stokes equations, subject to the continuity equation, are solved iteratively with the Navier equations for the elastic material. In a specified domain, the flow equations are solved, followed by integrating the pressure and the stresses along the vessel wall. Upon obtaining the fluid forces F_1 and F_2, the displacement can then be obtained by solving the Navier equations in biquadratic elements using the Galerkin finite-element model. The updated vessel configuration enables us to solve the flow equations. The above procedures are repeated over each time increment until the vessel shows a negligible change in its configuration.

3. FINITE-ELEMENT MODELS

The finite-element method has been well accepted to be effective to tackle problems with complex geometries and equations with Neumann-type boundary conditions. These attributes motivated us to use it to simulate the flow in a compliant vessel. In the present mixed finite-element context, we introduce the Sobolev space $\mathscr{H}_0^1(\Omega)$ for the velocity vector and the constrained space $\mathscr{L}_0^2(\Omega)$ for the pressure. Solutions are then sought for $\underline{u} \in \mathscr{H}_0^1(\Omega)$ and $p \in \mathscr{L}_0^2(\Omega)$ from the weak statement for the Navier–Stokes equations in moving co-ordinates. The test functions $\underline{w} \in \mathscr{H}_0^1(\Omega) \times \mathscr{H}_0^1(\Omega)$ and $q \in \mathscr{L}_0^2(\Omega)$ are used for equations governing the vector and scalar fields, respectively. To eliminate the troublesome pressure mode, we employ here the biquadratic polynomial, N_i, to approximate $\underline{u}$ and the bilinear polynomial, M_i, to approximate p since this variable setting accommodates the inf–sup (or div–stability) condition [29–31].

The time derivative term is, as before, approximated using the following second-order time-stepping scheme:

$$\frac{\mathrm{d}\phi}{\mathrm{d}t}\bigg|_j = \frac{1}{2\,\Delta t}(3\phi_j^{n+2} - 4\phi_j^{n+1} + \phi_j^n) \tag{23}$$

The simulated Galerkin solutions are formally second-order accurate in time and space for cases carried out in uniform grids.

Numerical prediction of physical conservation laws on moving meshes requires calculating u_g and v_g shown in Equations (9)–(10). Both the surface conservation law (SCL), which requires that each cell should be closed by its surfaces, and the volume conservation law

(VCL), which states that the volumetric increment of a moving cell must be equal to the summation of the volumetric increases along its surfaces that enclose the volume, must be taken into account in this regard. According to the terminology of Thomas and Lombard [22], we call the combination of SCL and VCL the GCL. In mathematical terms, SCL and VCL are expressed, respectively, below [32]:

$$\oint_B \underline{a}\,d\underline{s} = 0 \tag{24}$$

$$\frac{\partial V}{\partial t} = \oint_B \bar{\underline{w}}\,d\underline{s} = 0 \tag{25}$$

In the above, $\underline{s}$ represents the area in the outward normal direction of the boundary surface B that encloses the time-varying material volume V. As for vectors $\underline{a}$ and $\bar{\underline{w}}$, they represent the direction of a uniform flow in a non-moving mesh and a specified boundary velocity vector for B.

While two laws given in (24) and (25) are easily derived in the continuous sense, their discrete counterparts may not always be trivially satisfied. In discrete sense, any violation of GCL will produce errors in the flow field. Error of this type will cause the solution accuracy to deteriorate in two ways. An erroneous of discrete SCL will miscreant the convection velocity, while the non-satisfaction of discrete VCL will cause mass to accumulate or diminish from the numerically produced sources and sinks, respectively. While errors of these kinds have been reported, they are not addressed in many previous calculations. Instead, erroneous flow predictions owing to non–satisfaction of the discrete GCL were attributed to other sources. To close the Galerkin finite-element analysis in moving meshes, we have to provide values of grid velocities shown in (9)–(10). By integrating the GCL condition in its differential description and employing the divergence theorem, we are led to obtain the GCL condition in its integral description, namely, Equation (25). In other words, gird velocities are calculated under the following GCL constraint condition

$$\frac{1}{\sqrt{g}}\frac{\partial \sqrt{g}}{\partial t} = \nabla \underline{u}_{\mathrm{g}} \tag{26}$$

where $\sqrt{g}$ represents the determinant of the Jacobian matrix between fixed and moving co-ordinates.

There are several ways of moving nodes from their previous locations to the updated ones over each time step. In this study, we assume that $(u_{\mathrm{g}}, v_{\mathrm{g}})$ remains unchanged in magnitude as well as in direction from the previous location at $(x^{\mathrm{old}}, y^{\mathrm{old}})$ to the updated location at $(x^{\mathrm{new}}, y^{\mathrm{new}})$. To ensure that the geometric quantities satisfy the VCL and SCL and, thus, the GCL, we calculate u_{g} and v_{g} simply by

$$u_{\mathrm{g}} = \frac{x^{\mathrm{new}} - x^{\mathrm{old}}}{\Delta t} \tag{27a}$$

$$v_{\mathrm{g}} = \frac{y^{\mathrm{new}} - y^{\mathrm{old}}}{\Delta t} \tag{27b}$$
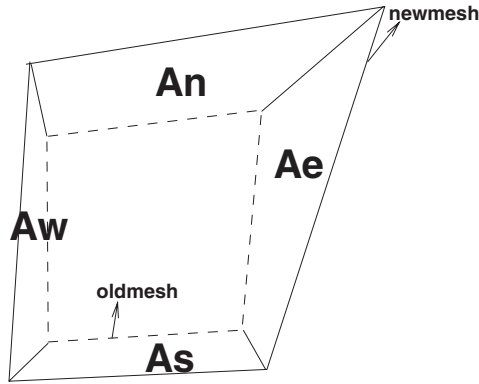
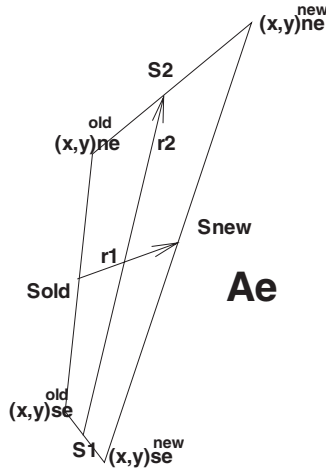Figure 1. Schematic of the movement of a representative mesh.

Figure 2. Schematic of the notations given in Equation (28).

The proof will be given below. Referring to Figure 1, which illustrates the movement of an old cell to its updated configuration. Denote A_e, A_w, A_s and A_n as the areas at the east, west, south and north sides of the old cell. Take A_e as an example; its area can be calculated from

$$A_e = \tfrac{1}{4}(\mathbf{S}_1 + \mathbf{S}_2) \times (\mathbf{S}^{new} + \mathbf{S}^{old}) \tag{28}$$

where $\mathbf{S}_1$, $\mathbf{S}_2$, $\mathbf{S}^{new}$ and $\mathbf{S}^{new}$ are schematic in Figure 2. Substitution of grid co-ordinates into (28) leads to

$$A_e = \tfrac{1}{4}((\delta x_{ne} + \delta x_{se})(\delta y_e^{new} + \delta y_e^{old}) - (\delta y_{ne} + \delta y_{se})(\delta x_e^{new} + \delta x_e^{old})) \tag{29}$$

where $\delta x_i = x_i^{new} - x_i^{old}$ ($i = \text{ne, se, e}$) and $\delta y_i = y_i^{new} - y_i^{old}$ ($i = \text{ne, se, e}$). Similarly, one can have A_s, A_w and A_n and, thus, can calculate the left-hand side of (25) from $1/\Delta t$ ($V^{new} -$

Table I. The computed L_2-error norms for displacements governed by elastic equations (15)–16).

Time	d_1 L_2-error norm	d_2 L_2-error norm
0.5	0.7693×10^{-8}	0.1298×10^{-7}
1.0	0.1113×10^{-7}	0.6656×10^{-8}
1.5	0.1335×10^{-7}	0.2987×10^{-8}
2.0	0.1129×10^{-7}	0.9524×10^{-8}

$V^{\mathrm{old}})(\equiv 1/\Delta t(A_{\mathrm{e}}+A_{\mathrm{s}}+A_{\mathrm{w}}+A_{\mathrm{n}}))$. We then proceed to calculate the right-hand side of Equation (25). Take the east side as an example; we have

$$\int_{\mathrm{e}} \underline{u}_{\mathrm{g}}\, \mathrm{d}\underline{s} = \int_{\mathrm{e}} u_{\mathrm{g}}\, \mathrm{d}s_y - \int_{\mathrm{e}} v_{\mathrm{g}}\, \mathrm{d}s_x = (\bar{u}_{\mathrm{g}})_{\mathrm{e}}(\bar{s}_y)_{\mathrm{e}} - (\bar{v}_{\mathrm{g}})_{\mathrm{e}}(\bar{s}_x)_{\mathrm{e}} \tag{30}$$

In the above, the superscript '−' denotes the average operator. It is found that Equations (29)/Δt and (30) are identical provided that

$$(\bar{u}_{\mathrm{g}})_{\mathrm{e}} = \frac{1}{2\,\Delta t}\,(\delta x_{\mathrm{ne}} + \delta x_{\mathrm{se}}) \tag{31a}$$

$$(\bar{v}_{\mathrm{g}})_{\mathrm{e}} = \frac{1}{2\,\Delta t}\,(\delta y_{\mathrm{ne}} + \delta y_{\mathrm{se}}) \tag{31b}$$

This means that GCL is satisfied if the grid velocities are computed according to (27) and (28).

To verify that the present finite-element model is applicable to simulate the fluid flow on moving grids, we have solved the variable transport equation and Navier–Stokes equations, which are all amenable to analytical solution, with success [33]. In the following, we will justify the finite-element model developed to solve the elastic equations for the time-varying displacement vector. Given $\underline{F}=\mathrm{e}^{-t}((x^2y^2 - 6y^2 - 8xy - 2x^2),\ (x^2y^2 - 6x^2 - 8xy - 2y^2))$, Equations (15)–(16) were solved subject to the boundary conditions. At $t=0$, we uniformly discretized the domain in $0\leqslant x,y\leqslant1.0$, resulting in a mesh with a resolution of 11×11. Calculation terminated at $t=2$ with a time increment set at $\Delta t=10^{-3}$. At $\rho_w=G=\lambda=1$, the exact displacement vector is easily shown to be identical to the specified velocity vector $\underline{u}=\mathrm{e}^{-t}x^2y^2\,(-1,-1)$. The prediction errors are cast in their L_2-norm for d_1 and d_2. As Table I shows, the present finite-element code can be applied with confidence to analyse the linearly elastic equation.

We also validated the finite-element code developed to simulate the elastic equation in cylindrical co-ordinates. The material properties remained the same as those considered in the previous case. Subject to the boundary conditions, the exact displacements were derived as $d_1=d_2=\mathrm{e}^{-t}x^2y^2$ provided that $F_1=\mathrm{e}^{-t}(x^2y^2 - 6y^2 - 12xy - 4x^2)$ and $F_2=\mathrm{e}^{-t}(x^2y^2 - 9x^2 - 8xy - 2y^2)$. The unit square domain $0\leqslant r,x\leqslant1$ was uniformly discretized to have 11×11 mesh points. The computed L_2-error norms, tabulated in Table II, confirmed that the present finite-element formulation for solving the elastic equations is second-order accurate in space.

Table II. The computed L_2-error norms for displacements governed by elastic equations cast in cylindrical co-ordinates.

Time	d_1 L_2-error norm	d_2 L_2-error norm
0.5	0.7693×10^{-8}	0.1298×10^{-7}
1.0	0.1113×10^{-7}	0.6628×10^{-8}
1.5	0.1335×10^{-7}	0.2987×10^{-8}
2.0	0.1129×10^{-7}	0.9524×10^{-8}

Table III. A comparison of computed and exact solutions at six chosen radial locations.

r Position (mm)	Exact	Numerical
5	0.0001610259	0.0001610257
5.2	0.0001572590	0.0001572588
5.4	0.0001538628	0.0001538626
5.6	0.0001507974	0.0001507973
5.8	0.0001480288	0.0001480287
5.6	0.0001455273	0.0001455271

We then validated the elastic finite-element code, developed in cylindrical co-ordinates, by virtue of the problem studied previously by Xu and Collins [28]. The tube under investigation has a thickness of 1 mm, an inner radius $r_i = 5$ mm and an outer radius $r_o = 6$ mm. To make the elastic equations amenable to exact solutions, we assumed that the tube length is long enough so that we can specify zero gradient boundary condition in the axial direction. Under these circumstances, the thick-walled tube displacement could be analytically derived in the radial direction as follows [34]:

$$d_r = \frac{r_i \bar{p}}{r(r_o^2 - r_i^2)E}[(1 + \bar{v})r_o^2 + (1 - \bar{v})r^2] \tag{32}$$

In the above, $\bar{p} = 2688$ Pa. This calculation was carried out at a Young's modulus of 5×10^5 Pa, a density of 10^3 kg/m^3, and a Poisson ratio of 0.49. We performed finite-element calculations in a domain having 11×201 mesh points. It is seen from Table III that the simulated solutions agree perfectly with the exact solution given in (32).

4. COMPUTED RESULTS

With the above excellent agreement between the simulated and analytic solutions, we will now consider channel flow subject to a moving indentation. This problem, schematically shown in Figure 3, has been experimentally calibrated [35] and numerically simulated [36–38]. The channel wall is rigid everywhere except at the indentation, which is placed downstream of the channel inlet. The indentation, made of a thick and stiff rubber membrane, changes its shape with the upward-and-downward moving piston. The maximum movement of the indented wall
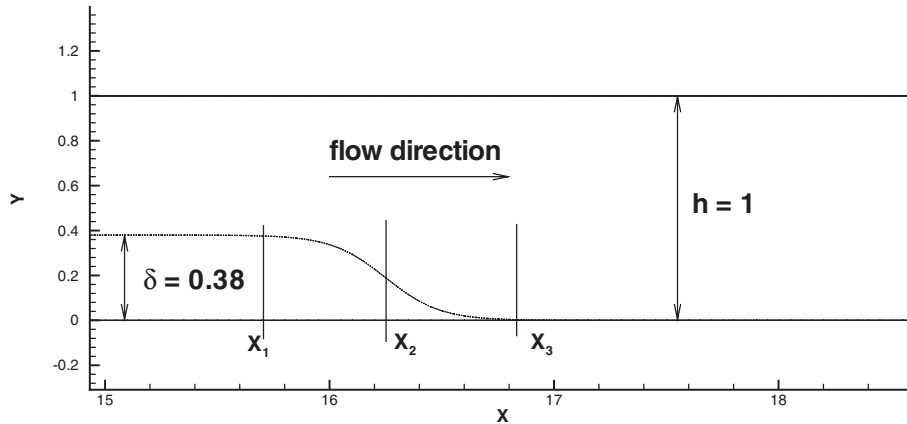
Figure 3. Schematic of the indented wall.

is $\delta = 0.38$ and is schematic in Figure 3. The configuration of the indented wall is algebraically represented by

$$y(x) = \begin{cases} 0.19h \left(1 - \cos\left(\frac{2\pi t}{T}\right)\right); & 0 \leqslant x \leqslant x_1 \\ 0.085h \left(1 - \cos\left(\frac{2\pi t}{T}\right)\right)(1 - \tanh(a(x - x_2))); & x_1 < x \leqslant x_3 \\ 0; & x > x_3 \end{cases} \tag{33}$$

In the above, $h(=1)$ and $T(=1)$ denote the channel height and the oscillation period. Other parameters intended for representing the time-varying indented wall are chosen as $a = 4.14$, $x_1 = 4h$, $x_2 = 5.25h$ and $x_3 = 6.5h$.

A fully developed velocity is specified at the inlet. The truncated outlet is far downstream of the indentation with a length of 40 so that the exit flow becomes fully developed again with vanishing values of v and $\partial u/\partial x$. At $t = 0$, the fully developed flow is solved with no indentation movement. The Reynolds number considered in this case is 100, which is obtained by choosing the channel height H as the reference length and the average entrance velocity $\bar{U}$ as the characteristic velocity. The case under investigation has a Strouhal number $St = Hf/\bar{U} = 0.03$, where f denotes the oscillating frequency of the moving piston. The time step chosen in this study is $\Delta t = 0.01$ and the mesh used for the present analysis has 21×551 points, which are non-uniformly distributed in the channel. To resolve the flow details, grids are clustered near the channel wall and in regions downstream of the indentation. At each time, the boundary grids are prescribed according to the moving indentation while the interior grids are re-distributed according to the grid velocities.

To give a global picture of the flow development in this partly indented channel, we plot first the instantaneous streamlines at ten chosen dimensionless times, starting from $t = 0.2$ and terminating at $t = 1.1$ with an increment of $\Delta t = 0.1$. As Figure 4 shows, the flow immediately downstream of the indentation is configured with a single eddy structure in the early stage of flow development. As time goes by, a second separated eddy forms on the opposite side of the channel wall. Later on, another smaller and weaker eddy forms on the channel floor. Such a vortex-shedding-like flow is reproduced as that observed experimentally by Pedley and

U$_c$ = 50   Re = 100

t = 0.2

t = 0.3

t = 0.4

t = 0.5
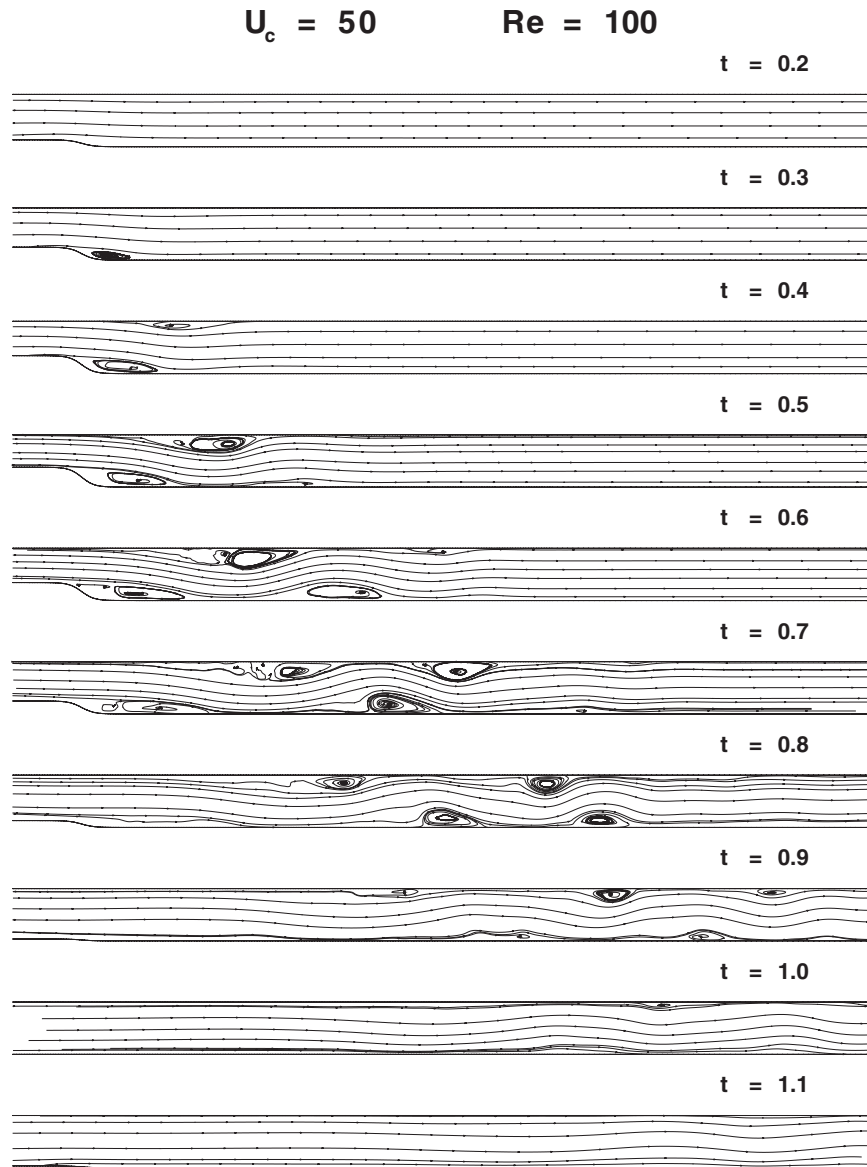
t = 0.6

t = 0.7

t = 0.8

t = 0.9

t = 1.0

t = 1.1

Figure 4. The computed time-varying streamlines.

Stephanoff [35], and numerically by Ralph and Pedley [36] and Rosenfield *et al.* [38]. The time-evolving vortex shedding phenomenon can be seen also in the pressure contours shown in Figure 5.

In order to demonstrate the applicability of the present flow/structure finite-element code, we have performed flow simulation in a finite-length elastic tube [28]. The tube with a length of 5 cm and a thickness of 1 mm has inner and outer diameters with the values of 10 and
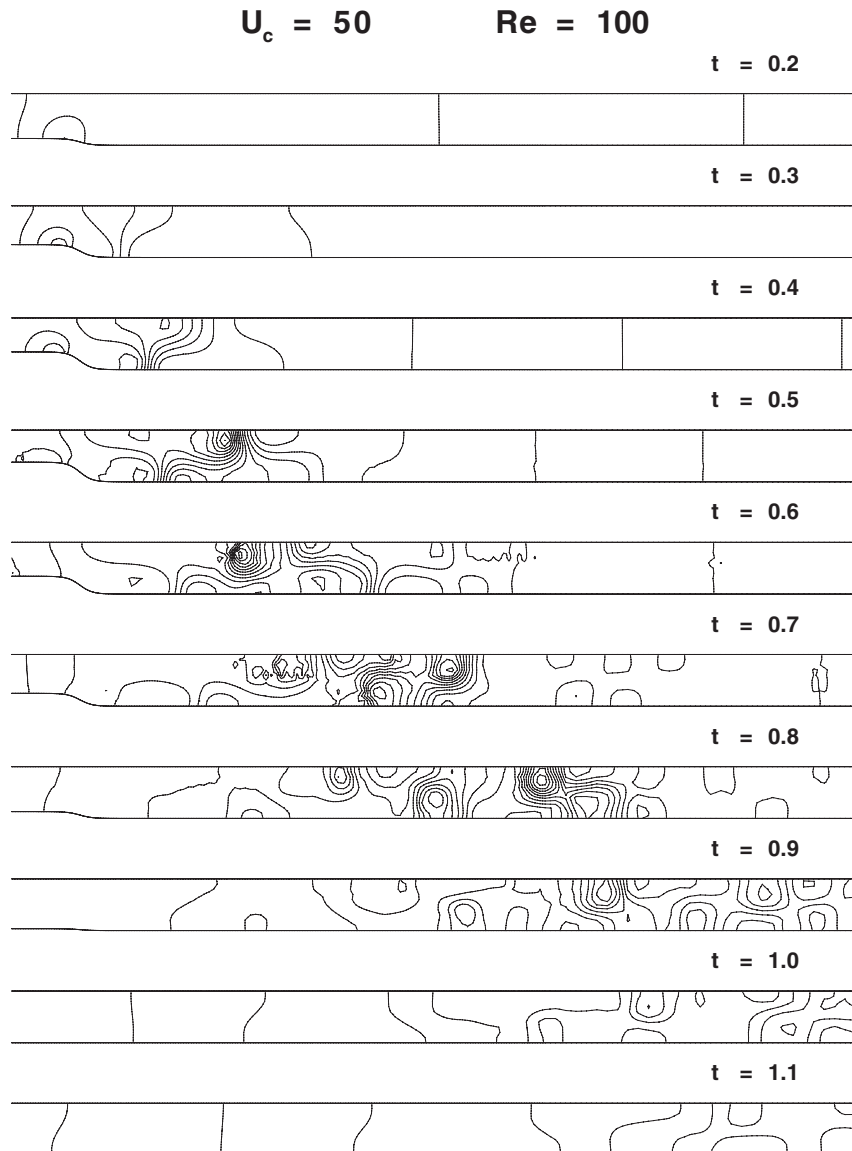
Figure 5. The computed time-varying pressure contours.

12 mm, respectively. In this study, both ends of the tube were assumed to be fixed. In the radial direction we divided the linearly elastic tube into seven fluid elements and two solid elements. In the axial direction there are 20 elements. At the vessel inlet, the pressure varied harmonically according to $\partial p / \partial x = -A \exp(int)$, where the amplitude A and the frequency chosen in this study are 200 and 2π, respectively.
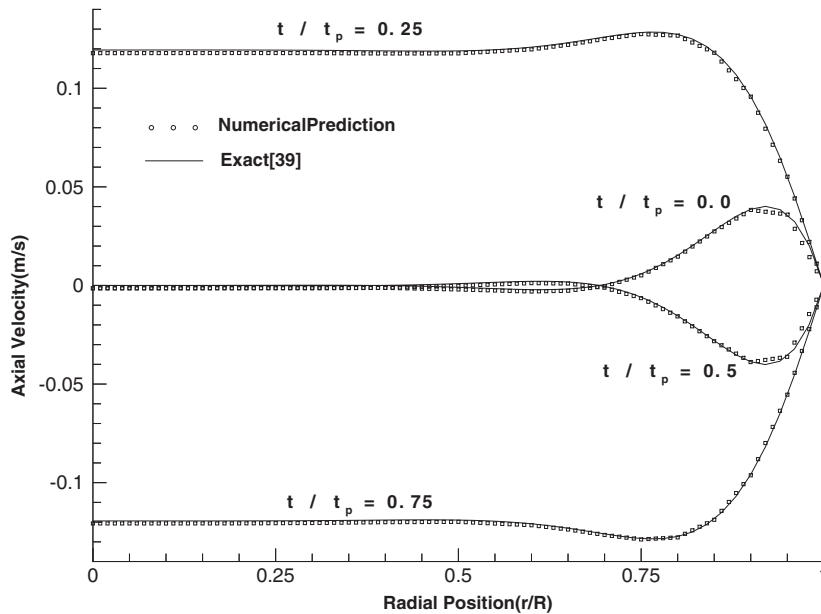
Figure 6. Analytical and predicted axial velocity profiles for transient flow in a compliant tube.

Given the initial condition, we had iteratively analysed this problem since the wall position at the updated time was unknown. Within each time step $\Delta t = 0.01$, we estimated the vessel position based on the currently available grid velocities. This is followed by carrying out the Navier–Stokes calculations to obtain the pressure that will be applied at the mostly updated domain boundary. We then solved for the elastic equations to update the vessel configuration. In the new physical domain, we proceeded to solve the flow equations. The above iterative procedures were repeated until the specified tolerances on the vessel displacement were obtained. Within each time step, less than eight iterations are needed to reach convergence in the fluid–wall iterative process. Following the above coupled fluid/solid solution procedures, we could obtain the axial velocity. The simulated axial velocities at four arbitrarily chosen times show a good agreement between the prediction and the analytical data given in Reference [39] as well as in Figure 6.

5. CONCLUDING REMARKS

In this paper, a GCL-satisfying finite-element model has been presented in moving meshes for the prediction of flow in a domain bounded partly by an elastic boundary. Working equations are cast in ALE description, which involves a grid velocity vector, so as to adapt to the flow in time-varying physical domain. We applied the Galerkin finite-element method to obtain a second-order spatially accurate solution and the second-order accurate time-stepping method for the time derivative terms. The proposed model for solving the flow equations in moving grids has been theoretically verified. In addition, the finite-element model developed to solve

the Navier equations for elastic media has been theoretically verified. Results have also been presented for the flow in a vessel, where part of its rigid/elastic surface bounding the physical flow region is allowed to move.

REFERENCES

1. Taylor CA, Hughes TJR, Zarins CK. Computational investigations in vascular disease. *Computers in Physics* 1996; **10**(3):224–232.
2. de Hart J, Cacciola G, Schreurs PJG, Peters GWM. A three-dimensional analysis of a fibre-reinforced aortic valve prosthesis. *Journal of Biomechanics* 1998; **31**:629–638.
3. Quarteroni A, Tuveri M, Veneziani A. Computational vascular fluid dynamics: problems, models and methods. *Computing and Visualization in Science* 2000; **2**:163–197.
4. Peskin C, McQueen D. A three-dimensional computational method for blood flow in the heart—1 immersed elastic fibers in a viscous incompressible fluid. *Journal of Computational Physics* 1989; **81**(2):372–405.
5. Kim J, Kim D, Choi H. An immersed-boundary finite-volume method for simulations of flow in complex geometries. *Journal of Computational Physics* 2001; **171**:132–150.
6. Glowinski R, Pan TW, Periaux J. A fictitious domain method for Dirichlet problem and applications. *Computer Methods in Applied Mechanics and Engineering* 1994; **111**:283–303.
7. Leveque RJ, Li Z. The immersed interface method for elliptic equations with discontinuous coefficients and singular sources. *SIAM Journal of Numerical Analysis* 1994: **31**:1019–1044.
8. Donea J. An arbitrary Lagrangian–Eulerian finite element method for transient fluid–structure interactions. *Computer Methods in Applied Mechanics and Engineering* 1982; **33**:689–723.
9. Hughes TJR, Hulbert GJ. Space–time finite element methods for elasto-dynamics: formulations and error estimates. *Computer Methods in Applied Mechanics and Engineering* 1988; **66**:339–363.
10. Hughes TJR, Liu WK, Zimmerman TK. Lagrangian–Eulerian finite element formulation for incompressible viscous flow. *Computer Methods in Applied Mechanics and Engineering* 1981; **29**:329–349.
11. Bernardi C, Maday Y, Patera AT. Domain decomposition by the mortar element method. In *Asymptotic and Numerical Methods for PDEs with Critical Parameters*, vol. 384. Kaper HG, Garbey M. (eds), *NATO ASI Series C: Mathematical and Physical Sciences*. Kluwer: Dordrecht, 1993, pp. 169–186.
12. Ben Belgacem F, Maday Y. The mortar fiinite element method for the three dimensional finite elements. *RAIRO Analyse Numerique* 1997; **31**:289–302.
13. Hansbo P. The characteristic streamline diffusion method for the time-dependent incompressible Navier–Stokes equations. *Computer Methods in Applied Mechanics and Engineering* 1992; **99**:171–186.
14. Behr M, Tezduyar TE. Finite element solution strategies for large-scale flow simulations. *Computer Methods in Applied Mechanics and Engineering* 1994; **112**:3–24.
15. Chen S, Doolen GD. Lattice Boltzmann method for fluid flows. *Annual Review of Fluid Mechanics* 1998; **30**:329–361.
16. Esmaeeli A, Tryggvason F. Direct numerical simulation of bubbly flow, Part 2, moderate Reynolds number arrays. *Journal of Fluid Mechanics* 1999; **385**:325–358.
17. Hu HH, Patankar NA, Zhu MY. Direct numerical simulation of fluid-solid systems using the arbitrary Lagrangian–Eulerian technique. *Journal of Computational Physics* 2001; **169**:427–462.
18. Formaggia L, Nobile F. A stability analysis for the arbitrary Lagrangian Eulerian formulation with finite elements. *East–West Journal of Numerical Mathematics* 1999; **7**:105–132.
19. Satoru O, Tomiko I. A method for computing flow fields around moving bodies. *Journal of Computational Physics* 1987; **69**:49–68.
20. Schouten JA. *An Introduction to Tensor Analysis and its Geometrical Applications. Ricci–Calculus*. Springer: Berlin, 1954.
21. Trulio JG, Trigger KR. *Numerical solution of the one-dimensional hydrodynamic equations in an arbitrary time-dependent coordinate system*. University of California Lawrence Radiation Laboratory Report UCLR–6522, 1961.
22. Thomas PD, Lombard CK. Geometric conservation law and its application to flow computations on moving grids. *AIAA Journal* 1979; **17**(10):1030–1037.

23. Demirdizic I, Peric M. Space conservation law in finite volume calculation of fluid flow. *International Journal for Numerical Methods in Fluids* 1983; **8**:1037–1050.
24. Koobus B, Farhat C. Second-order implicit schemes that satisfy the GCL for flow computations on dynamic girds. *AIAA–paper*, 1997; 1–14.
25. Lesoinne M, Farhat C. Geometric conservation laws for aeroelastic computations using unstructured dynamic meshes. *AIAA Paper 95-1709*, *12th AIAA CFD Conference*, *San Diego*, *CA*, *June 19–22*. American Institute of Aeronautics and Astronautics: New York, 1995.
26. Zhang H, Reggio M, Trèpanier Y, Camarero R. Geometric form of the GCL for moving meshes and its implementation in CFD schemes. *Computers and Fluids* 1993; **22**(1):9–23.
27. Ladyzhenskaya O. *The Mathematical Theory of Viscous Incompressible Flow*. Gordon and Breach: New York, 1969.
28. Xu YY, Collins MW. Numerical modelling of blood flow in compliant arteries and arterial bifurcations. In *Bio-fluid Mechanics*. Power H (ed.). Computational Mechanics Publications: Souampton, 1995; 55–94.
29. Brezzi F, Douglas J. Stabilized mixed methods for the Stokes problem. *Numerische Mathematik* 1988; **53**:225–235.
30. Babuska I. The finite element method with Lagrangian multipliers. *Numerische Mathematik* 1973; **20**:179–192.
31. Brezzi F. On the existence, uniqueness and approximation of saddle point problem analysis from Lagrangian multipliers, RAIRO. *Analytical Numerics* 1974; **8**(R2):129–151.
32. Zhang H, Reggio M, Trèpanier JY, Camarero R. Discrete form of the GCL for moving meshes and its implementation in CFD schemes. *Computers and Fluids* 1993; **22**(1):9–23.
33. Sheu TWH, Chen HYH. A transient analysis of incompressible fluid flow in vessels with moving boundaries. *International Journal for Numerical Methods in Heat and Fluid Flow* 1999; **9**(8):833–846.
34. Love AEH. *A Treatise on the Mathematical Theory of Elasticity*. Cambridge University Press: Cambridge, MA, 1952.
35. Pedley TJ, Stephanoff KD. Flow along a channel with a time-dependent indentation in one wall: the generation of vorticity waves. *Journal of Fluid Mechanics* 1985; **160**:337–367.
36. Ralph ME, Pedley TJ. Flow in a channel with a moving indentation. *Journal of Fluid Mechanics* 1988; **190**:87–112.
37. Demirdizic I, Peric M. Finite volume method for prediction of fluid flow in arbitrarily shaped domains with moving boundaries. *International Journal for Numerical Methods in Fluids* 1990; **10**:771–790.
38. Rosenfield M, Kwak D, Vinokur M. A fractional step solution method for the unsteady incompressible Navier–Stokes equations in generalized coordinate systems. *Journal of Computational Physics* 1991; **94**(1):102–137.
39. Womersley JR. The mathematical analysis of the arterial circulation in a state of oscillatory motion. *WADC–TR*, 56–614, Wright Air Developmant Center, 1957.